

Entanglement entropies of the $J_1 - J_2$ Heisenberg antiferromagnet on the square lattice

Nicolas Laflorencie, David J. Luitz, and Fabien Alet

Laboratoire de Physique Théorique, IRSAMC, Université de Toulouse, CNRS, 31062 Toulouse, France

(Dated: July 24, 2018)

Using a modified spin-wave theory which artificially restores zero sublattice magnetization on finite lattices, we investigate the entanglement properties of the Néel ordered $J_1 - J_2$ Heisenberg antiferromagnet on the square lattice. Different kinds of subsystem geometries are studied, either corner-free (line, strip) or with sharp corners (square). Contributions from the $n_G = 2$ Nambu-Goldstone modes give additive logarithmic corrections with a prefactor $n_G/2$ independent of the Rényi index. On the other hand, corners lead to additional (negative) logarithmic corrections with a prefactor l_q^c which does depend on both n_G and the Rényi index q , in good agreement with scalar field theory predictions. By varying the second neighbor coupling J_2 we also explore universality across the Néel ordered side of the phase diagram of the $J_1 - J_2$ antiferromagnet, from the frustrated side $0 < J_2/J_1 < 1/2$ where the area law term is maximal, to the strongly ferromagnetic regime $-J_2/J_1 \gg 1$ with a purely logarithmic growth $S_q = \frac{n_G}{2} \ln N$, thus recovering the mean-field limit for a subsystem of N sites. Finally, a universal subleading constant term γ_q^{ord} is extracted in the case of strip subsystems, and a direct relation is found (in the large- S limit) with the same constant extracted from free lattice systems. The singular limit of vanishing aspect ratios is also explored, where we identify for γ_q^{ord} a regular part and a singular component, explaining the discrepancy of the linear scaling term for fixed width *vs.* fixed aspect ratio subsystems.

PACS numbers: 02.70.Ss, 03.67.Mn, 75.10.Jm, 05.10.Ln

I. INTRODUCTION

Entanglement properties of interacting quantum spin systems have recently attracted a lot of interest. In particular, great attention is paid to the universal information carried by bipartite entanglement measures such as the Rényi entanglement entropies (EEs) defined by

$$S_q = \frac{1}{1-q} \ln \text{Tr} (\hat{\rho}_\Omega)^q, \quad (1.1)$$

where $\hat{\rho}_\Omega$ is the reduced density matrix of a given subsystem Ω (see Fig. 1) computed in the ground-state wavefunction. Note that the special limit of $q \rightarrow 1$ corresponds to the standard von Neumann EE given by $S_1 = -\text{Tr} \rho_\Omega \ln \rho_\Omega$ and is always implicitly understood whenever we refer to $q = 1$. As a general result, at $T = 0$ the Rényi EEs follow an area law^{1,2} in dimension d

$$S_q = a_q L^{d-1} + \dots \quad (1.2)$$

where L^{d-1} is the size of the boundary between subsystem Ω and the rest, and the ellipses are subleading corrections. Such corrections have been shown to carry universal information about topological order³⁻⁶, or the presence of Nambu-Goldstone modes associated to the breaking of a continuous symmetry⁷⁻¹⁰. In the latter case, Metlitski and Grover (MG)⁷ have derived the following analytical expression in the case of smooth boundaries (no corner), as for instance depicted for $d = 2$ in Fig. 1 (a) for $L \times \ell$ strip subsystems:

$$S_q = a_q L^{d-1} + \frac{n_G}{2} \ln \left(\frac{\rho_s}{v} L^{d-1} \right) + \gamma_q^{\text{ord}}, \quad (1.3)$$

where ρ_s is the stiffness, v the velocity of the n_G Nambu-Goldstone modes, and γ_q^{ord} a universal geometric constant. In the case of subsystems having sharp corners, as

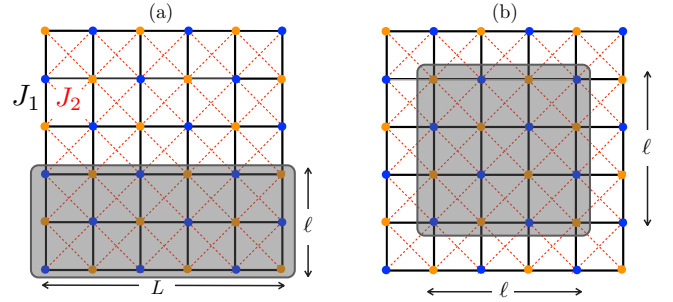


Figure 1. Schematic picture for the $L \times L$ square lattice $J_1 - J_2$ antiferromagnet on a torus with 2 types of entanglement bipartitions: (a) rectangular strip of extent $L \times \ell$ with no corners and (b) square of extent $\ell \times \ell$ with four $\pi/2$ corners. In all this work, we assume periodic boundary conditions in both directions.

depicted in Fig. 1 (b), it is expected that⁷:

$$S_q = a_q L^{d-1} + \frac{n_G}{2} \ln \left(\frac{\rho_s}{v} L^{d-1} \right) + n_G \sum_c l_q^c(\varphi_c) \ln \left(\frac{L}{a} \right) + \gamma_q^{\text{ord}}, \quad (1.4)$$

where a is a non-universal length scale, and the corner contribution depends on n_G , the Rényi parameter q , and the number of corners c of angle φ_c . The contributions $l_q^c(\varphi_c)$ from each corner come from the (free) Goldstone modes and can be computed, following the work of Casini and Huerta¹¹ on scalar field theory, by the numerical solution of a set of non-linear differential equations, valid for $\varphi_c \in [0, \pi]$ ($l_q(\varphi) = l_q(2\pi - \varphi)$) and $q \in \mathbb{N} \setminus \{1\}$.

Previous works have explored the scaling of the entanglement entropy in ground-states of systems that break

continuous symmetries in the thermodynamic limit. Subleading logarithmic corrections arising from the Goldstone modes have been observed in quantum Monte Carlo simulations of finite spin systems^{12–14}, even though the prefactor of this correction did not perfectly agree with the prediction $n_G/2$, until a very recent large-scale, low-temperature quantum Monte Carlo (QMC) investigation by Kulchytskyy *et al.*⁹ for the 2d XY model and $q = 2$. Logarithmic corrections have also been observed in finite-size SW calculations⁸ (similar to the ones presented in this manuscript), but not with a high-enough precision to again ascertain the prediction, except for the case a line-shaped subsystem for which the prefactor $n_G/2$ could be recovered assuming further subleading corrections¹⁰ (see also the recent work Ref. 15). The existence of logarithmic corrections have also been discussed based on a phenomenological picture of the tower of low-lying states in the symmetry-broken phase of antiferromagnets¹². Logarithmic corrections due to corner contributions have on the other hand been identified and calculated precisely in free lattice systems¹¹, broken continuous symmetries systems¹² as well as for various critical points using QMC, cluster expansions or tree tensor network techniques^{12–14,16–24}. In a recent work²⁵, predictions for the universality of corner contributions in various theories are also provided. Finally, Kulchytskyy *et al.*⁹ could also compute with QMC the subleading constant correction γ_2^{ord} in the 2d XY model, finding a good agreement with the prediction of MG in Ref. 7.

In this paper, we provide a systematic high-precision study of the universal nature of three subleading terms of the Rényi EE appearing in Eq. (1.4) for a generic model of quantum antiferromagnetism in two dimensions ($d = 2$). This is achieved using a large- S semi-classical approach, the modified linear spin-wave (SW) theory, where the rotational SU(2) symmetry, while practically broken, is artificially restored for finite size systems^{26,27}. We focus on the $J_1 - J_2$ spin- S antiferromagnet defined on a bipartite $L \times L$ square lattice by the following Hamiltonian

$$\mathcal{H} = J_1 \sum_{\langle ij \rangle} \mathbf{S}_i \cdot \mathbf{S}_j + J_2 \sum_{\langle\langle ij \rangle\rangle} \mathbf{S}_i \cdot \mathbf{S}_j + h \sum_i (-1)^i S_i^z, \quad (1.5)$$

where \mathbf{S} are spin- S operators, interactions act between nearest neighbours $\langle ij \rangle$ and second nearest neighbours $\langle\langle ij \rangle\rangle$ along the diagonals of a square lattice (see Fig. 1), and h is an external staggered field. We impose periodic boundary conditions in all directions. At $h = 0$ this model spontaneously breaks the SU(2) symmetry at zero temperature in the thermodynamic limit, and displays Néel order for $J_2 < J_2^c$, with $J_2^c \rightarrow J_1/2$ for $S \rightarrow \infty$ ²⁸. The restoration of zero sublattice magnetization in finite systems is made possible by tuning the small staggered field $h^*(L)$ such that on any site $\langle S_i^z \rangle = 0$. As first done in Refs. 8 and 10, this allows to correctly compute Rényi EEs on finite systems. Here we make a systematic and extensive study across the full Néel regime $-\infty < J_2 < J_2^c$

for various subsystem shapes and sizes in order to characterize contributions from (i) Nambu-Goldstone modes, (ii) corners, (iii) frustration effects $J_2/J_1 > 0$, and (iv) geometric effects appearing through the universal constant γ_q^{ord} in Eq. (1.3).

Let us briefly summarize our main results. Using a large- S approach, we have numerically extracted the three subleading corrections in the scaling of EEs Eq. (1.4) with $n_G = 2$ for SU(2) antiferromagnets. Universality has been tested in the entire Néel ordered regime of the $J_1 - J_2$ Heisenberg model Eq. (1.5) for various S , even in the frustrated regime where QMC is inapplicable. In the case of subsystems having sharp corners, small negative corner terms l_q^c are found, in perfect agreement with the predictions by Casini and Huerta for free scalar fields¹¹. The non-universal area-law term has also been studied as a function of the second neighbour coupling, showing remarkable behaviors both in the mean-field limit ($-J_2/J_1 \gg 1$) where it vanishes, and close to the frustrated critical point J_2^c where the area law prefactor strongly increases, while log corrections due to Nambu-Goldstone modes are still present. Furthermore, the additional geometric constant γ_q^{ord} , which depends on the subsystem aspect ratio ℓ/L , is extracted for various Rényi indices, and a simple relation with the free scalar field result is derived. We have also explored the limit of vanishing aspect ratios where a non-trivial slow singular behavior shows up as $\gamma_q^{\text{ord}}(\ell/L \ll 1) \rightarrow -\infty$.

The rest of the paper is organized as follows. In Section II we start by recalling the modified SW formalism for the $J_1 - J_2$ spin- S antiferromagnet, and how it can be used to compute the Rényi EEs. We then turn to the results for EEs in Section III where we discuss several aspects: we first describe numerical diagonalization results, which can be conveniently performed up to subsystems of $\lesssim 10^5$ sites, for various shapes of subsystems including strips (Sec. III A and Fig. 1a) and squares (Fig. 1b), with a particular focus on the corner contributions (Sec. III B) and their dependence on the Rényi parameter q . In Section III C the dependence on the second neighbour coupling J_2 is studied, focussing on the non-universal area law prefactor a_q . In Section IV we discuss the constant term γ_q^{ord} which is compared to the field-theory prediction of MG in Sec. IV A. An interesting connection to the free scalar field result is achieved in Sec. IV B. We further explore the singular limit of vanishing aspect ratios in Sec. IV C using quasi-analytical results for single and double line subsystems where translation symmetry inside the subsystem allows to get an explicit expression for S_q . Finally we summarize and discuss our results in Section V. Details of spin-wave calculations are provided in Appendix A, analytical results for the mean-field limit $-J_2/J_2 \gg 1$ are presented in Appendix B, and an analytical derivation for one-dimensional subsystems is given in Appendix C.

II. MODIFIED SPIN-WAVE APPROACH

A. Dyson-Maleev transformation and Bogoliubov diagonalization

We use the Dyson-Maleev formalism^{29,30} to map spin operators onto bosonic ones. For sites on sublattice A of the square lattice:

$$S_i^z = S - b_i^\dagger b_i, \quad S_i^+ = (2S - b_i^\dagger b_i) b_i, \quad S_i^- = b_i^\dagger, \quad (2.1)$$

and for the sublattice B:

$$S_i^z = b_i^\dagger b_i - S, \quad S_i^+ = -b_i^\dagger (2S - b_i^\dagger b_i), \quad S_i^- = -b_i. \quad (2.2)$$

Truncating at $1/S$ order, the $J_1 - J_2$ Hamiltonian Eq. (1.5) becomes (up to a constant)

$$\begin{aligned} \mathcal{H} = & \sum_i (h + 4S[J_1 - J_2]) b_i^\dagger b_i \\ & + \sum_{\langle ij \rangle} S J_2 (b_i^\dagger b_j + b_j^\dagger b_i) - \sum_{\langle ij \rangle} S J_1 (b_i b_j + b_j^\dagger b_i^\dagger). \end{aligned} \quad (2.3)$$

After a Fourier transformation, it reads

$$\mathcal{H} = \sum_{\mathbf{k}} A_{\mathbf{k}} (b_{\mathbf{k}}^\dagger b_{\mathbf{k}} + b_{-\mathbf{k}}^\dagger b_{-\mathbf{k}}) + B_{\mathbf{k}} (b_{\mathbf{k}}^\dagger b_{-\mathbf{k}}^\dagger + b_{\mathbf{k}} b_{-\mathbf{k}}), \quad (2.4)$$

with

$$A_{\mathbf{k}} = 2S J_2 \cos k_x \cos k_y + 2S(J_1 - J_2) + \frac{h}{2} \quad (2.5)$$

$$B_{\mathbf{k}} = -S J_1 [\cos k_x + \cos k_y]. \quad (2.6)$$

The quadratic part of the above Hamiltonian can be diagonalized via a standard Bogoliubov transformation:

$$b_{\mathbf{k}} = u_{\mathbf{k}} \alpha_{\mathbf{k}} - v_{\mathbf{k}} \alpha_{-\mathbf{k}}^\dagger, \quad b_{\mathbf{k}}^\dagger = u_{\mathbf{k}} \alpha_{\mathbf{k}}^\dagger - v_{\mathbf{k}} \alpha_{-\mathbf{k}}. \quad (2.7)$$

The quasiparticle operators $\alpha_{\mathbf{k}}$ and $\alpha_{\mathbf{k}}^\dagger$ satisfy bosonic commutation relations provided $u_{\mathbf{k}}^2 - v_{\mathbf{k}}^2 = 1$, and diagonalize (2.4) if

$$u_{\mathbf{k}}^2 = \frac{1}{2} \left(\frac{A_{\mathbf{k}}}{\sqrt{A_{\mathbf{k}}^2 - B_{\mathbf{k}}^2}} + 1 \right) \quad (2.8)$$

$$v_{\mathbf{k}}^2 = \frac{1}{2} \left(\frac{A_{\mathbf{k}}}{\sqrt{A_{\mathbf{k}}^2 - B_{\mathbf{k}}^2}} - 1 \right). \quad (2.9)$$

In terms of Bogoliubov quasi-particles, the $J_1 - J_2$ Hamiltonian takes the simpler form

$$\mathcal{H} = \sum_{\mathbf{k}} \Omega_{\mathbf{k}} \alpha_{\mathbf{k}}^\dagger \alpha_{\mathbf{k}} + \text{constant}, \quad (2.10)$$

with the SW excitation spectrum $\Omega_{\mathbf{k}} = 2\sqrt{A_{\mathbf{k}}^2 - B_{\mathbf{k}}^2}$ (this spectrum is illustrated in Appendix A). In the vicinity of the two minima at $\mathbf{k} = (\pi, \pi)$ and $(0, 0)$, the dispersion is linear, with a velocity

$$v_{\text{sw}} = 2\sqrt{2S} \sqrt{J_1(J_1 - 2J_2)}, \quad (2.11)$$

which is defined only on the AF side $J_2 < J_1/2$. The SW spectrum and velocity are illustrated in Fig. 13 and 14 of Appendix A.

In the thermodynamic limit, the continuous SU(2) symmetry of the original $J_1 - J_2$ Hamiltonian can be spontaneously broken, with the two associated Nambu-Goldstone modes at $\mathbf{k} = (\pi, \pi)$ and $(0, 0)$. The corresponding staggered magnetization order parameter is given at the $1/S$ order by

$$\begin{aligned} m_{\text{AF}} &= \lim_{h \rightarrow 0} \lim_{N \rightarrow \infty} \langle S_i^z \rangle \\ &= S + \frac{1}{2} - \frac{1}{8\pi^2} \int_{\text{Bz}} d^2\mathbf{k} \frac{A_{\mathbf{k}}}{\Omega_{\mathbf{k}}}. \end{aligned} \quad (2.12)$$

In Appendix A, this expression is evaluated numerically to obtain the range of parameter space where Néel order is expected from this SW treatment.

B. Spin-Wave theory for finite size systems

The above SW approach assumes a classical ordered state as a starting point. This does not allow for a correct study of finite size effects since the spin rotational symmetry has to remain unbroken on finite-size lattices. In order to repair this, adding a staggered magnetic field to the quantum antiferromagnet allows to artificially restore zero sub-lattice (SW-corrected) magnetization, as originally proposed in Refs. 26 and 27. This will turn crucial to capture the subleading scaling terms in the entanglement entropy.

In this approach, one imposes that for any given finite size sample $\langle S_i^z \rangle = 0 \quad \forall i$, which yields a staggered field h^* such that the number of Holstein-Primakoff bosons $\langle n \rangle = S$. This leads to

$$\sum_{\mathbf{k}} \frac{A_{\mathbf{k}}(h^*)}{\Omega_{\mathbf{k}}(h^*)} = N(2S + 1). \quad (2.13)$$

This regularizing field is very small and scales rapidly to zero with the system size⁸. Indeed, one can rewrite Eq. (2.13) as follows

$$N(2S + 1) - \sum_{\mathbf{k} \neq \mathbf{k}_0} \frac{A_{\mathbf{k}}(h^*)}{\Omega_{\mathbf{k}}(h^*)} = 2 \frac{A_{\mathbf{k}_0}(h^*)}{\Omega_{\mathbf{k}_0}(h^*)}, \quad (2.14)$$

where $\mathbf{k}_0 = (0, 0)$ and (π, π) are the singular modes where the dispersion vanishes in the absence of staggered field. The contributions from these two modes, divergent in the limit $h^* \rightarrow 0$, are similar:

$$\frac{A_{\mathbf{k}_0}}{\Omega_{\mathbf{k}_0}} = \frac{4S J_1 + h^*}{\sqrt{h^*(h^* + 8S J_1)}}. \quad (2.15)$$

Defining

$$m^*(N, h^*) = S + \frac{1}{2} - \frac{1}{2N} \sum_{\mathbf{k} \neq \mathbf{k}_0} \frac{A_{\mathbf{k}}(h^*)}{\Omega_{\mathbf{k}}(h^*)} \quad (2.16)$$

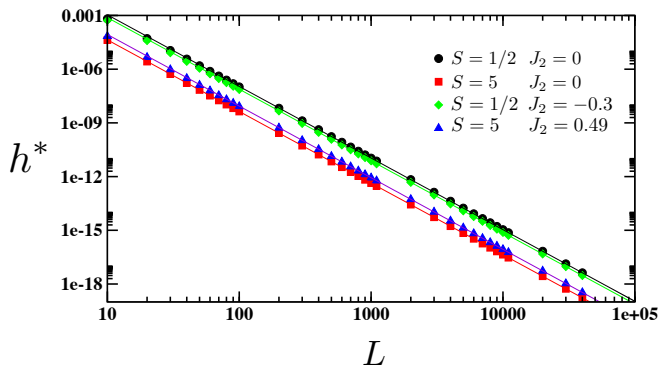


Figure 2. Regularizing staggered magnetic field h^* in the J_1 - J_2 antiferromagnet such that SW corrected magnetization vanishes.

we obtain a self-consistent equation for h^*

$$h^* = 4SJ_1 \left[\frac{1}{\sqrt{1 - \left(\frac{1}{Nm^*}\right)^2}} - 1 \right]. \quad (2.17)$$

In the limit $N \gg 1$, $m^* \rightarrow m_{\text{AF}}$, and we have

$$h^* \simeq \frac{2SJ_1}{m_{\text{AF}}^2} \frac{1}{N^2}. \quad (2.18)$$

As seen below, it is essential to determine the actual value of $h^*(L)$ with a high precision in order to compute accurately various finite size correlations. Since the field h^* gets rapidly very small with increasing system sizes, we resort to a multiple precision evaluation of the self-consistent equation Eq. (2.17). In Fig. 2 we present the result showing the behavior of $h^*(L)$ for some representative values of J_2 and S . In all cases, the staggered field vanishes very fast and is well described by Eq. (2.18) at large enough L .

Interestingly this small staggered field opens a gap in the excitation spectrum

$$\begin{aligned} \Delta^* &\simeq \sqrt{2SJ_1 h^*} \\ &\simeq \frac{2SJ_1}{m_{\text{AF}}} \frac{1}{N} \end{aligned} \quad (2.19)$$

which scales in the same way as the Anderson tower of states³¹. Therefore, the excitation spectrum has linearly dispersing Nambu-Goldstone (SW) modes with a level spacing $\sim 1/L$ and a tower of states like finite size gap $\sim 1/L^2$ produced by the symmetry restoring staggered field.

We use this modified finite-size SW approach to compute the entanglement entropy as detailed below. In order to show that it reproduces fairly well the physics of finite-size systems, we also compare in Appendix A results for the finite-size structure factor for $S = 1/2$ and various $J_2 < 0$ to the ones obtained with the exact QMC method.

C. Entanglement entropy

As the diagonalized Hamiltonian Eq. (2.10) is non-interacting, Wick's theorem eases the computation of entanglement entropy, which can nicely be extracted from the correlation matrix³², an object which contains all two-body correlations within a block of sites. For completeness, we recapitulate here the essential formulae.

We first need to define single particle Green's function $\langle b_i^\dagger b_j \rangle = -\frac{\delta_{ij}}{2} + f_{ij}$ and $\langle b_i b_j \rangle = g_{ij}$, with

$$\begin{aligned} f_{ij} &= \frac{1}{2N} \sum_{\mathbf{k}} \frac{A_{\mathbf{k}} \cos[\mathbf{k} \cdot (\mathbf{r}_i - \mathbf{r}_j)]}{\Omega_{\mathbf{k}}} \\ g_{ij} &= -\frac{1}{2N} \sum_{\mathbf{k}} \frac{B_{\mathbf{k}} \cos[\mathbf{k} \cdot (\mathbf{r}_i - \mathbf{r}_j)]}{\Omega_{\mathbf{k}}}. \end{aligned} \quad (2.20)$$

We remark that $g_{ij} = 0$ ($f_{ij} = 0$) if i and j belong to the same (different) sublattice(s).

The entanglement entropy of a region Ω containing N_Ω sites can then be extracted³³⁻³⁵ from the eigenvalues ν_l^2 of the $N_\Omega \times N_\Omega$ correlation matrix \mathbf{C}

$$C_{ij} = \sum_{i' \in \Omega} (f_{ii'} + g_{ii'})(f_{i'j} - g_{i'j}) \quad (2.21)$$

where $i, j \in \Omega$. Due to the sublattice properties of f and g , we have that $C_{ij} = C_{ji}$ if i and j belong to the same sublattice, $C_{ij} = -C_{ji}$ otherwise.

The Rényi entanglement entropy is obtained as³²

$$S_q = \frac{1}{q-1} \sum_{l=1}^{N_\Omega} \ln \left[\left(\nu_l + \frac{1}{2} \right)^q - \left(\nu_l - \frac{1}{2} \right)^q \right], \quad (2.22)$$

which for $q = 1$ reads

$$S_1 = \sum_{l=1}^{N_\Omega} \sum_{\epsilon = \pm 1} \epsilon \left(\nu_l + \frac{\epsilon}{2} \right) \ln \left(\nu_l + \frac{\epsilon}{2} \right), \quad (2.23)$$

and for $q = \infty$

$$S_\infty = \sum_{l=1}^{N_\Omega} \ln \left(\nu_l + \frac{1}{2} \right). \quad (2.24)$$

As first shown by Srednicki³⁶, Callan and Wilczek³⁷, the entropy of a free massless bosonic field obeys a strict area law, which is what we observe (data not shown) in the absence of the regularizing staggered field h^* . However, as we will see below, the finite staggered field which opens a finite size gap $\sim 1/N$ leads to an additive logarithmic correction proportional to the number of Goldstone bosons.

III. RESULTS FOR EE

A. Strip geometry

Let us start with the case of an $L \times \ell$ strip subsystem embedded in an $L \times L$ torus, as depicted in Fig. 1

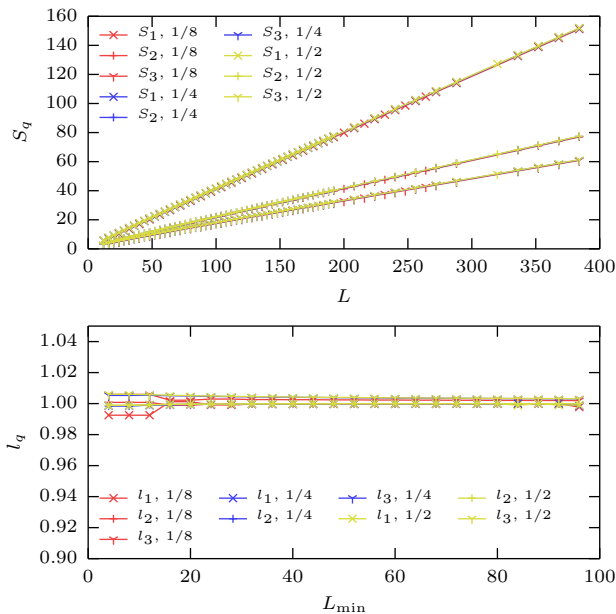


Figure 3. Entanglement Rényi entropies for the strip subsystem with different aspect ratios ℓ/L (upper panel) and fit results for the prefactor l_q of the logarithmic scaling term as a function of the minimal system size L_{\min} included in the fit (lower panel). The results displayed here have been obtained for $S = \frac{1}{2}$ and $J_2 = 0$. Clearly, $l_q = 1$ independent of q and the aspect ratio of the subsystem.

(a). This geometry has no corner and we therefore expect the expression Eq. (1.3) to hold. Results obtained from the exact diagonalization of the correlation matrix \mathbf{C} for systems up to $\sim 10^5$ lattice sites are shown in the upper panel of Fig. 3 where the Rényi entropies for $q = 1, 2, 3$ are displayed for three representative aspect ratios $\ell/L = 1/2, 1/4, 1/8$. Note that for this strip geometry, translation symmetry of the subsystem is used, allowing the diagonalization procedure to reach large sizes. This plot clearly demonstrates the area law behavior $S_q \sim a_q L$ since the dominant scaling behavior does not depend on the number of subsystem sites but only on its perimeter $2L$, which is independent of the aspect ratio of the subsystem. The properties of the area law prefactor a_q will be analyzed in detail in Sec. III C, and the universal additive constant γ_q from Eq. (1.3) in Sec. IV.

Here, we want to focus on the logarithmic correction associated to the breaking of $SU(2)$ rotational symmetry with $n_G = 2$ Nambu-Goldstone modes, expected to be $\frac{n_G}{2} \ln L$. This correction is believed to be universal as it should not depend on the geometry and only reflect the nature of the continuous symmetry which is broken in the ground state^{7,9,10}. Therefore, we perform fits to the general scaling ansatz

$$S_q(L) = a_q L + l_q \ln L + b_q + c_q/L + d_q/L^2, \quad (3.1)$$

over various fit ranges $[L_{\min}, L_{\max}]$. Results for l_q are

plotted in the lower panel of Fig. 3 for various values of the Rényi parameter and several aspect ratios. For $q = 1, 2$ we clearly observe that $l_q = 1$ over basically the whole range of L_{\min} , whereas for larger values of q , the convergence is relatively slow as these results are to our experience hampered by more severe finite size effects. Nevertheless, the resulting l_q is already very close to 1 and the deviation decreases slowly as L_{\min} is increased. This leads us to the conclusion that, within our SW approach, we find $l_q = n_G/2 = 1$ to be independent on q and the aspect ratio of the subsystem, in perfect agreement with the field theoretical result by MG⁷.

B. Square subsystems: corner contributions

In addition to the breaking of continuous symmetries, logarithmic corrections to the area law can also be caused by geometry: In particular, logarithmic corrections induced by sharp corners of the subsystem have been discussed in several works^{11,13,14,16–18,20–22,25,38,39}. The prefactor of the logarithmic corner correction term is expected to be universal for all systems with the same type of symmetry breaking/phase transition. However, such corrections are quite difficult to capture with QMC since the prefactor is very small. Together with the contributions coming from Nambu-Goldstone modes Eq. (1.4), we expect a total correction of the form

$$n_G \left(\sum_c l_q^c(\varphi_c) + \frac{1}{2} \right) \ln L, \quad (3.2)$$

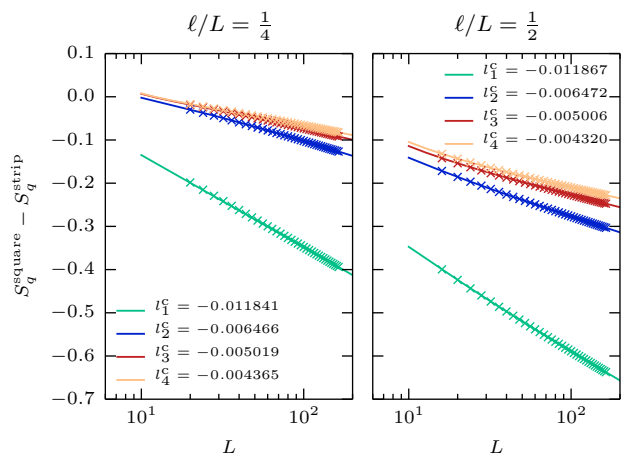


Figure 4. Difference of entanglement entropies for the $S = 1/2$ $J_2 = 0$ Heisenberg antiferromagnet of square and strip subsystems having the same boundary length. The remaining dominant scaling term is the logarithmic term which stems from the corners of the square subsystem. We show fits (full lines) to the form $8l_q^c(\pi/2) \ln(L) + b_q + c_q/L + d_q/L^2$. SW results (symbols) are shown for two different aspect ratios ℓ/L for $q = 1, 2, 3$ and 4.

	$q = 1$	$q = 2$	$q = 3$	$q = 4$
CH ¹¹	-0.0118	-0.0064	-0.0051	
This work	-0.0118(1)	-0.0064(1)	-0.0050(1)	-0.0043(1)

Table I. Prefactor $l_q^c(\pi/2)$ of the corner logarithmic correction obtained after fitting data in Fig. 4. A comparison with data of Casini and Huerta (CH)¹¹ is also given.

where the sum is taken over all sharp corners inside the subsystem making an angle φ_c . Here we aim at numerically extracting $l_q^c(\pi/2)$ for a square subsystem (panel (b) of Fig. 1), expected to coincide with the result of a free scalar field¹¹. To do so, we work with a $L \times L$ torus and subtract the entropies of a periodic (corner-free) strip of size $L \times \ell$ from those of a $L/2 \times L/2$ square. Both subsystems having the same area law $\sim 2L$, independent of the strip aspect ratio ℓ/L , and identical logarithmic corrections due to Goldstone modes, we therefore expect the leading term of this difference to be given only by the corner log contribution:

$$S_q^{\text{square}} - S_q^{\text{strip}} = 8l_q^c(\pi/2) \ln L + \dots \quad (3.3)$$

Numerical results are plotted in Fig. 4 where we clearly see that the above difference Eq. (3.3) is indeed dominated by a logarithmic scaling which allows us to extract $l_q^c(\pi/2)$. Small variations of the results for different aspect ratios of the strips (see left and right panels of Fig. 4) can be used as a measure of the error due to finite size effects and fitting procedure. Our results are displayed in Table I where we compare to the free-field results by Casini and Huerta (CH)¹¹.

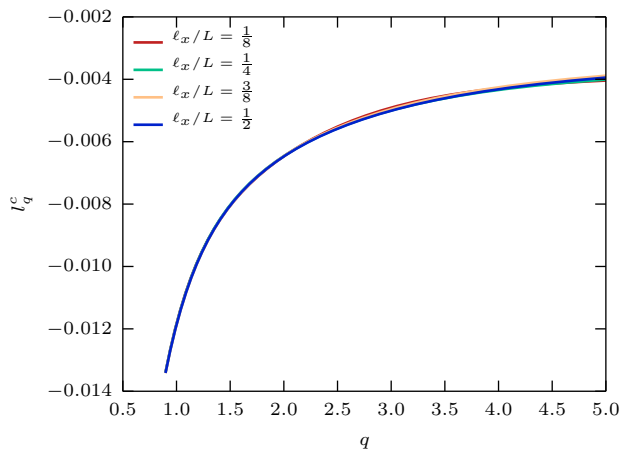


Figure 5. Logarithmic contribution of a $\frac{\pi}{2}$ corner of the subsystem as a function of q . This result is obtained for $J_2 = 0$ and $S = \frac{1}{2}$ by subtracting the entanglement entropy of a strip subsystem with the same perimeter as the square subsystem with 4 $\frac{\pi}{2}$ corners and fitting to the same form as shown in Fig. 4 for different aspect ratios of the strip. Up to slight deviations for larger Rényi indices q due to finite size effects, the results do not depend on the aspect ratio.

Interestingly, we can also study the dependence on the Rényi index for non-integer values of q . In Fig. 5 we show $l_q^c(\pi/2)$ versus the Rényi parameter q for four different aspect ratios. For q not too large, the estimates obtained after fitting our numerical data (see caption of Fig. 4), are clearly independent of the aspect ratio, as expected. This non-trivial q -dependence for a free scalar field can be compared to recent numerical results for $O(1)$ and $O(2)$ Wilson-Fisher critical points²¹, featuring qualitatively similar behaviors.

C. J_2 -dependence and area law prefactor

Besides universal contributions arising from Nambu-Goldstone modes and corners, we now study the dominant part which governs the entanglement growth with the subsystem area. As already discussed in the beginning of the paper, the $J_1 - J_2$ spin- S Heisenberg model on the square lattice is Néel ordered for $J_2/J_1 < 0.5$ in the large S limit (see Appendix A and Fig. 15 for the critical value of J_2 as a function of S). Scanning across the entire Néel ordered regime, we have performed fits to the form Eq. (3.1) for various values of the second neighbor coupling J_2 and spin S for the strip geometry (corner-free) with a $1/8$ aspect ratio. Shown in Fig. 6, the area law coefficient a_q displays a quite remarkable behavior. First, the results appear to be almost independent of the spin size S . Then, as expected from the mean-field limit $J_2/J_1 \rightarrow -\infty$ (see Refs. 40 and 41 and Appendix B), a_q goes to zero in the limit $-J_2/J_1 \gg 1$. This is because the ground-state becomes more and more classical, with

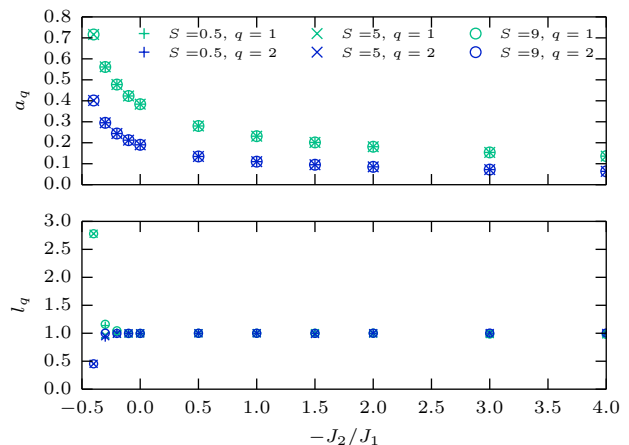


Figure 6. Top: Area law coefficients a_q for $q = 1, 2$ (extracted for an aspect ratio $\ell/L = 1/8$) as a function of the next neighbor coupling J_2/J_1 . Approaching the critical point in the frustrated regime ($J_2 > 0$) the area law coefficient grows rapidly. Bottom: Prefactor l_q of the log correction in Eq. (1.3) due to the two Goldstone modes of the antiferromagnet. The deviation of l_q from 1 close to the critical point in the frustrated regime reveals the limitation of the SW approximation.

a very low entanglement. However, less is known when frustration is turned on, and we observe a rapid growth of the area law term when the critical point is approached, a feature also observed for the unfrustrated Heisenberg bilayer¹⁴. Note that the validity of the SW calculation can be questioned when quantum fluctuations become large, approaching the critical point J_2^c . Nevertheless, we believe the results to be under control if $1 - m_{\text{AF}}/S \ll 1$, a condition which can be checked in Fig. 15 of Appendix A. Moreover, as long as the logarithmic term in the entanglement entropies scaling is still present and equal to one (due to the two Nambu-Goldstone modes, as shown in the bottom panel of Fig. 6 thus confirming the universality across the ordered phase), we believe the SW approximation correctly captures the behavior of EE. In practice, we start to see a deviation of l_q from unity only for the very last points at $J_2/J_1 \geq 0.3$ in Fig. 6.

IV. UNIVERSAL ADDITIVE CONSTANT γ_q^{ord}

A. Direct extraction from large- S data

Following MG⁷, a universal additive constant $\gamma_q^{\text{ord}}(\ell/L)$, depending on the aspect ratio ℓ/L of a strip, appears in the Rényi EE scaling Eq. (1.3). Nevertheless, there is also a non-universal term involving the spin stiffness and the SW velocity in Eq. (1.3). It is therefore much easier to work in the $S \rightarrow \infty$ limit of the $J_1 - J_2$ Heisenberg Hamiltonian where ρ_s and v are known exactly. In such a limit and having shown above that the logarithmic prefactor is exactly given by $l_q = n_G/2 = 1$

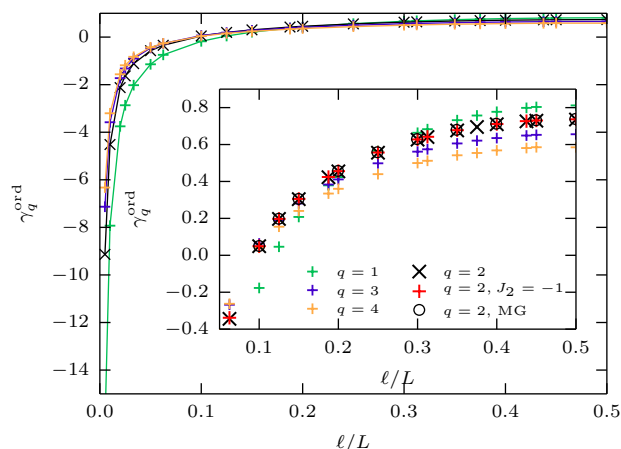


Figure 7. Universal additive constant $\gamma_q^{\text{ord}}(\ell/L)$ for different Rényi indices q as a function of the aspect ratio of the strip geometry for the $S = 100$ Heisenberg $J_1 - J_2$ antiferromagnet at $J_2 = 0$. The inset displays a zoom, showing that our result is in perfect agreement with the universal geometric constant obtained by MG⁷ for $q = 2$. Results for $J_2/J_1 = -1$ at $q = 2$, shown by red plus signs, agree perfectly with MG (black circles) and $J_2 = 0$ (black x), confirming universality.

(the corner contribution vanishes for this geometry), we expect the EE scaling for strips with an aspect ratio ℓ/L to be in the $S \gg 1$ limit

$$S_q = a_q L + \ln \left(S \sqrt{\frac{J_1 - 2J_2}{8J_1}} L \right) + \gamma_q^{\text{ord}}(\ell/L). \quad (4.1)$$

This large S expression has been used to fit our numerical SW data obtained for $S = 100$ and $J_2/J_1 = 0, -1$. Results for the additive constant $\gamma_q^{\text{ord}}(\ell/L)$ are plotted in Fig. 7 as a function of the aspect ratio ℓ/L for various Rényi parameters q . The agreement with the result extracted from Ref. 7 is excellent for $q = 2$. The universal character of $\gamma_q^{\text{ord}}(\ell/L)$ is also corroborated by the fact that our estimates do not depend on the values of the second neighbour coupling $J_2/J_1 = 0, -1$; the sole J_2 dependence being given by the two first terms in Eq. (4.1).

For the $S = 1/2$ Heisenberg model ($J_2 = 0$), while we have seen above that the logarithmic corrections are perfectly captured, a precise determination of the additional constant $\gamma_q^{\text{ord}}(\ell/L)$ is less obvious. Indeed, as shown in Fig. 8 for $q = 2$, using $\rho_s/v = 0.11675$ from previous $1/S$ estimates⁴³, the γ_2^{ord} estimates are close but do not agree with the $S = 100$ results. Taking instead the most recent QMC estimate⁴² for this ratio $\rho_s/v = 0.10882(4)$, the agreement is clearly better. We have also checked that results on $\gamma_q^{\text{ord}}(\ell/L)$ obtained by taking into account higher orders in $1/S$ from Ref. 43 give indeed an improvement over the $1/S$ order, but are not as good as the QMC result.

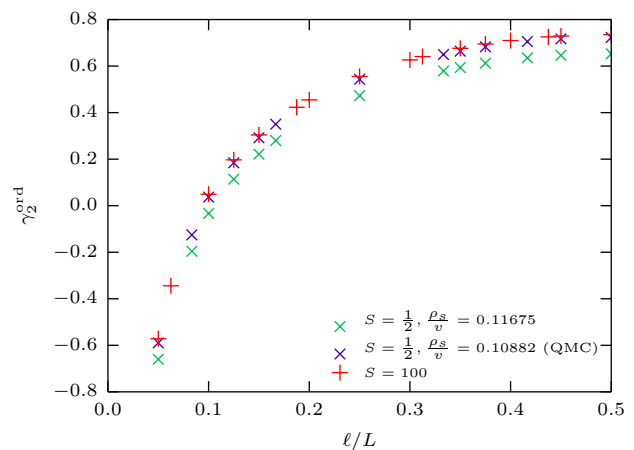


Figure 8. Results for $S = \frac{1}{2}$ and $J_2 = 0$ for γ_2^{ord} obtained from fits using rectangular subsystems with fixed aspect ratios. For $S = \frac{1}{2}$, we show two sets of results using slightly different estimates for ρ_s/v . Data shown in blue use $\rho_s/v = 0.10882(4)$ from the most recent QMC estimate⁴², while data shown in green use $\rho_s/v = 0.11675$ from a $1/S$ calculation⁴³. The use of the QMC result leads to a much better agreement with our $S = 100$ data.

B. Connection to the free scalar field result

In a (corner free) strip subsystem geometry with a finite aspect ratio ℓ/L , one expects for gapped free bosons with a very large correlation length $\xi \gg L$ the following subleading corrections to the area law⁷:

$$\Delta S_q = \frac{1}{2} \ln \left(\frac{\xi}{L} \right) + \gamma_q^{\text{free}}(\ell/L), \quad (4.2)$$

where $\gamma_q^{\text{free}}(\ell/L)$ is a universal geometric constant which depends non-trivially on both the Rényi parameter and the aspect ratio. By artificially gapping the linear SW Hamiltonian Eq. (2.4) with a very small staggered field h , the dispersion relation in the vicinity of its two minima reads

$$\Omega(\mathbf{k}) = \sqrt{8SJ_1h + 8S^2J_1(J_1 - 2J_2)|\mathbf{k}|^2}, \quad (4.3)$$

thus leading to

$$\xi = \sqrt{\frac{S(J_1 - 2J_2)}{h}}. \quad (4.4)$$

The correction due to the two minima becomes

$$\Delta S_q = \ln \left(\sqrt{\frac{S(J_1 - 2J_2)}{hL^2}} \right) + 2\gamma_q^{\text{free}}(\ell/L), \quad (4.5)$$

which is used to fit numerical SW results with a very small field $h = 10^{-18}$ to extract $\gamma_q^{\text{free}}(\ell/L)$, shown in Fig. 9.

Quite interestingly, from the above formulation we can infer a very simple and direct relation between γ_q^{ord} and γ_q^{free} . Indeed, in the large S limit the size-dependent

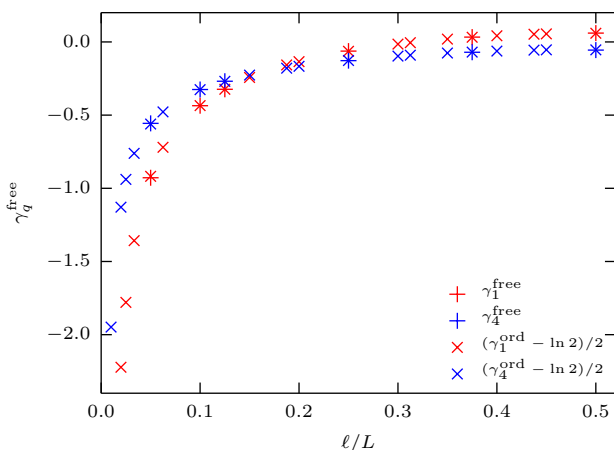


Figure 9. Universal additive constant $\gamma_q^{\text{free}}(\ell/L)$ for free bosons plotted against the aspect ratio of the strip subsystem. Linear SW results for the $S = 1/2$ Heisenberg antiferromagnet at $J_2 = 0$ are shown together with large- S estimates of γ_q^{ord} .

staggered field (added to artificially restore zero sublattice magnetization) takes the exact form $h^*(L) = \frac{2J_1}{SL^4}$. Plugging this into Eq. (4.5) yields

$$\gamma_q^{\text{ord SU}(2)} = 2\gamma_q^{\text{free}} + \ln 2, \quad (4.6)$$

which agrees with MG⁷, but only when $q = 2$. In Fig. 9, comparing γ_q^{free} to $(\gamma_q^{\text{ord SU}(2)} - \ln 2)/2$ for $q = 1, 4$ gives a perfect agreement for a wide range of aspect ratios.

One can also repeat the same argument for the XY model with only one Nambu-Goldstone mode¹⁰ to get

$$\gamma_q^{\text{ord U}(1)} = \gamma_q^{\text{free}} + \frac{5}{4} \ln 2. \quad (4.7)$$

The reason for the disagreement between our large S approach — expected to become unbiased in the limit $S \rightarrow \infty$ — and the result from Ref. 7 for γ_q^{ord} is not clear at the moment.

C. Limit of vanishing aspect ratio

In this section we shed light on the divergent behavior of γ_q^{ord} for small aspect ratios by calculating γ_q^{ord} in the extreme limit of $\ell/L \rightarrow 0$ using subsystems with a fixed number ℓ of lines and thus a varying aspect ratio as a function of L . In order to achieve this, we work with $S = 100$ at $J_2 = 0$, and we want to subtract all dominant terms, in particular the linear area law contribution $a_q L$.

Let us therefore start with a study of the dominant scaling contribution of S_q by plotting S_q/L vs. $1/L$ as displayed in Fig. 10. We show the area law behavior by plotting S_2/L vs. $1/L$ and an extrapolation $L \rightarrow \infty$, which guarantees to eliminate all subleading terms. The figure shows two sets of curves. In the first one, each curve corresponds to subsystems with a constant aspect ratio, such that γ_2^{ord} is a constant for each curve. These curves all yield identical area law prefactors $a_2^* = 0.190216(1)$ as expected.

The second set of curves shows results corresponding to a fixed number ℓ of lines in the subsystem (*i.e.* a ℓ -leg ladder), which implies that the aspect ratio of the subsystem is a function of L . The dominant linear prefactor a_q^ℓ found for the ℓ -leg ladder subsystem is different from the fixed aspect ratio value, which is approached only for $\ell \gg 1$. The reason for this discrepancy lies in the divergent behavior of γ_2^{ord} when ℓ/L tends to zero and the fact that the assumption that the only surviving term in the scaling of S_q/L at large sizes is the area law is no longer true. In fact, as the aspect ratio of the subsystem changes constantly, γ_q^{ord} seems to have a contribution that is linear in the inverse aspect ratio and hence leads to a shift or an effectively *changed area law prefactor*. As a next step, we will try to determine this contribution.

Fig 11 shows our data for γ_2^{ord} as obtained in Sec. IV multiplied by the aspect ratio $\frac{\ell}{L}$ as a function of the aspect ratio in order to extract the singular contribution γ_2^* as the intercept at vanishing aspect ratio. The data

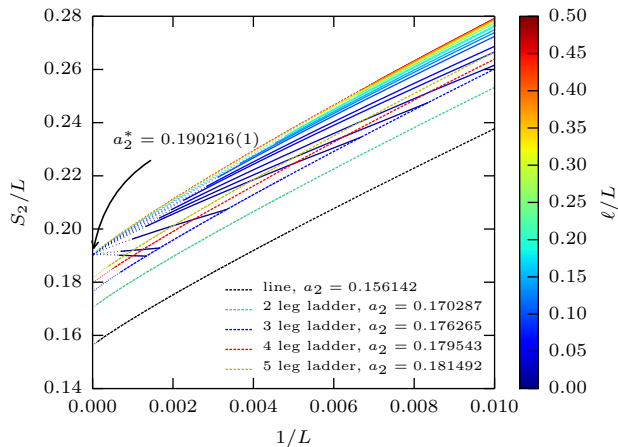


Figure 10. S_2/L vs. $1/L$ for the strip shaped subsystem with different aspect ratios (rainbow curves). SW data obtained for $S = 100$ and $J_2 = 0$. The dotted lines show an extrapolation for infinite system sizes which demonstrates that for all aspect ratios the leading scaling term is indeed an area law. We also show results for the line and 2, 3, 4 and 5 leg ladder subsystems (labeled lines) which clearly deviate significantly from this behavior. This discrepancy is caused by the singular behavior of γ_q^{ord} (and higher subleading terms), as the aspect ratio of these subsystems changes constantly with L and runs into the divergence of small aspect ratios (see text).

shows convincing evidence that this contribution indeed extrapolates to a nonvanishing value, which we determine by a cubic fit. With this information, we can now decompose γ_q^{ord} in a singular and a regular component:

$$\begin{aligned} \gamma_q^{\text{ord}}\left(\frac{\ell}{L}\right) &= \gamma_q^{\text{reg,ord}}\left(\frac{\ell}{L}\right) + \frac{L}{\ell}\gamma_q^*, \\ \lim_{\frac{\ell}{L} \rightarrow 0} \left(\frac{\ell}{L}\gamma_q^{\text{reg,ord}}\right) &= 0. \end{aligned} \quad (4.8)$$

For completeness, we provide a table of γ_q^* for other Rényi indices q in Tab. II.

In general, we can assume that other subdominant terms show pathologic behavior in the limit of vanishing (and non constant) aspect ratios, *i.e.* for fixed width ℓ subsystems, we will for the moment assume that they could produce a total correction to the area law of the form $\eta^* \frac{L}{\ell^2}$ in total. The scaling of the EE then reads:

$$\begin{aligned} S_q &= (a_q^* + \gamma_q^*/\ell + \eta_q^*/\ell^2) L \\ &+ \frac{n_G}{2} \ln\left(\frac{\rho_s}{v} L\right) + \gamma_q^{\text{reg,ord}} + \dots \end{aligned} \quad (4.9)$$

q	1	2	3	4
γ_q^*	-0.07677	-0.04579	-0.03530	-0.03123

Table II. Values of γ_q^* for different Rényi indices.

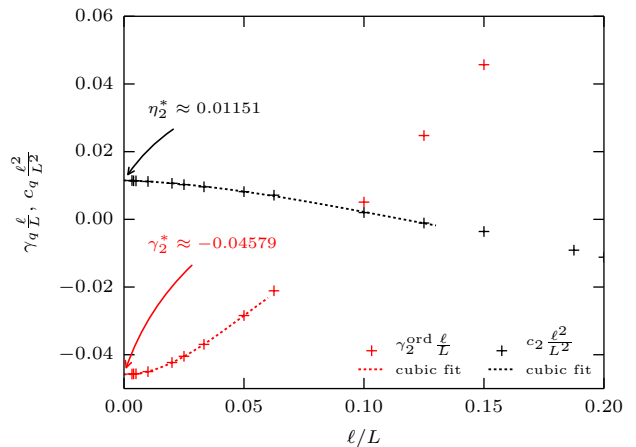


Figure 11. Singular contribution γ_2^* of $\gamma_2^{\text{ord}}(\frac{\ell}{L})$ (red) and singular contribution η_2^* of c_q (black). The dashed line corresponds to cubic fits for the smallest aspect ratios and are used to extract estimates of γ_2^* and η_2^* , given by the intercept at vanishing aspect ratio. γ_2^* corresponds to the contribution of γ_2 to the linear scaling of the entanglement entropy of fixed width subsystems. η_2^* is the linear scaling contribution stemming from the EE scaling term c_q/L .

Clearly, for fixed aspect ratio subsystems the terms γ_q^* and η_q^* become irrelevant for the area law for large system sizes. However, for fixed width subsystems, the effective linear (in L) scaling coefficient a_q^ℓ is in fact given by

$$a_q^\ell = a_q^* + \gamma_q^*/\ell + \eta_q^*/\ell^2. \quad (4.10)$$

We can therefore obtain (in the limit of large L) γ_q^{ord} from fixed width subsystems by subtracting several terms from S_q : Obviously we need to subtract $(a_q^\ell - \gamma_q^*/\ell) L$ to eliminate the linear contribution (note how this automatically takes care of the unknown terms η_q^*).

The second term that we have to subtract from the EE is the logarithmic term which is due to the spontaneous breaking of $SU(2)$ symmetry. We have argued above alongside with several works⁷⁻⁹ that its value is $n_G/2 = 1$ for the case of fixed aspect ratio subsystems and shown in Ref. 10 that this is also true for fixed width ℓ subsystems, such as the single line with $\ell = 1$, we therefore subtract the term $n_G/2 \ln(\frac{\rho_s}{v} L)$, taking also care of the constant stemming from ρ_s/v , that we know with great accuracy for the case of $S = 100$ at $J_2 = 0$.

Remaining subleading terms are expected to die off in the limit of $\ell/L \rightarrow 0$ and are therefore unimportant in the region of interest.

In total, for the limit of $L \rightarrow \infty$ and a fixed width ℓ of the subsystem, we obtain γ_q^{ord} through:

$$\gamma_q^{\text{ord}}\left(\frac{\ell}{L}\right) = S_q - (a_q^\ell - \gamma_q^*/\ell) L - \frac{n_G}{2} \ln\left(\frac{\rho_s}{v} L\right). \quad (4.11)$$

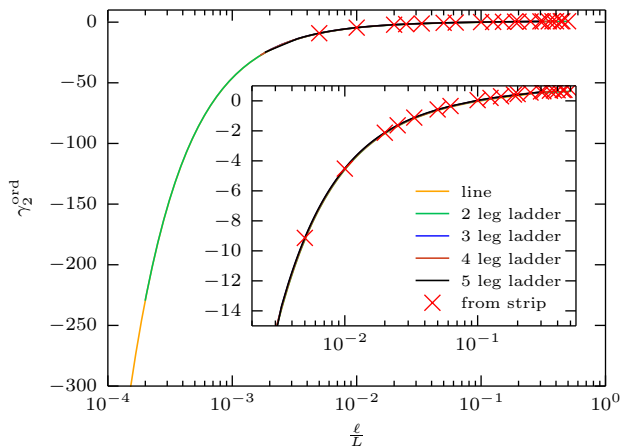


Figure 12. Data for γ_2^{ord} as obtained from fits for fixed aspect ratio subsystems (red x) shown together with the result of Eq. (4.11) for fixed width subsystems. The agreement is excellent, even for relatively large aspect ratios which correspond to small systems in the fixed width case. The inset shows a zoom. Lines are guides to the eye.

We can now apply Eq. (4.11) to calculate γ_q^{ord} in the small aspect ratio regime from fixed width subsystems of width ℓ . Fig. 12 shows our result in comparison the previously obtained values of γ_2^{ord} from fixed aspect ratio subsystems (strips). SW results for $\ell = 1$ and $\ell = 2$ are built on an analytical derivation (presented in Appendix C) obtained exploiting the fully symmetric nature of such subsystems. The perfect agreement of the results obtained with different methods and in particular the agreement of the results for different ℓ is a strong evidence for the reliability of this result and therefore demonstrates also the singular nature of γ_q^{ord} given by the singular component γ_q^* .

ℓ	a_q^ℓ	$a_q^* + \gamma_q^*/\ell + \eta_q^*/\ell^2$	$a_q^* + \gamma_q^*/\ell$
1	0.156142	0.155936	0.144426
2	0.170287	0.170199	0.167321
3	0.176265	0.176232	0.174953
4	0.179543	0.179488	0.178768
5	0.181492	0.181518	0.181058

Table III. Comparison of the directly obtained linear scaling factor a_q^ℓ of fixed width subsystems to the result obtained using the singular contributions γ_2^* and η_2^* from subdominant terms. The inclusion of η_q^* significantly improves the result and provides numerical evidence for the correctness of Eq. (4.10).

Can higher subleading terms generate corrections to the area law coefficient? It is certainly legal to assume that pathological behavior in the limit of $\ell/L \rightarrow 0$ is not only present in the scaling constant γ_q^{ord} but also in higher terms, such as c_q/L and d_q/L^2 . However, for them to modify the area law coefficient, they have to di-

verge much faster, *i.e.* as ℓ^2/L^2 for the case of c_q . In order to investigate this possibility, we plot $c_2 \frac{\ell^2}{L^2}$ in black in Fig. 11 and observe that a (small) nonzero contribution to the linear scaling in L is indeed present which we call η_2^* (here we will neglect the contributions to η from even higher terms, which are difficult to access through fits to numerical data). Let us finally plug all the information together and see if the singular contributions of subdominant terms can explain the discrepancy between a_q^* and a_q^ℓ observed in Fig. 10 by comparing in Tab. III results for a_q^ℓ as obtained from a direct fit to fixed width EEs and for $a_q^* + \gamma_q^*/\ell + \eta_q^*/\ell^2$. The left column shows the total linear scaling prefactor a_q^ℓ for fixed width subsystems as displayed in Fig. 10, while the rightmost column shows the fixed aspect ratio linear scaling prefactor a_q^* corrected by the singular contribution of γ_q^{ord} , giving reasonable agreement. The middle column takes into account the next subdominant singular contribution η_q^* from the term c_q/L as discussed above and reproduces the direct fit result to very high accuracy, thus providing strong evidence for the correctness of Eq. (4.10). We expect that even less dominant terms, such as d_q/L^2 will provide further corrections, which are relevant for small widths ℓ and should account for the remaining discrepancy, these terms are however very small and extremely difficult to extract numerically.

V. DISCUSSIONS AND CONCLUSIONS

In this work, we have performed a high-precision SW study of the $J_1 - J_2$ Heisenberg SU(2) antiferromagnet on the square lattice in order to investigate its quantum entanglement properties. Numerical calculations on finite size systems have been performed with an artificial restoration of zero sub-lattice magnetization using a small size-dependent staggered field $h^*(L)$. Several situations have been explored, and we have obtained finite size scaling results at large enough size such that the various terms appearing in the entanglement entropies have been precisely computed.

The universal logarithmic correction due to Nambu-Goldstone modes associated with the breaking of a continuous symmetry (SU(2) in the present case) are well captured, giving a correction perfectly fitted by $\frac{n_G}{2} \ln L$, independent of the Rényi index q . In the case of subsystem having sharp corners, additional (negative) logarithmic corrections have been precisely evaluated, in perfect agreement with scalar field theory predictions¹¹. The $J_1 - J_2$ model also offers a nice playground where we could check universality of the logarithmic term across the entire ordered regime but where we could further study the non-universal area law part which exhibits a non-trivial behavior, with a noticeable growth approaching the critical point in the frustrated regime. In the opposite limit of strong ferromagnetic second neighbor coupling, the mean-field limit is recovered with a vanish-

ing area law term and a smooth crossover to a purely logarithmic scaling of the entropies.

Part of this work was also devoted to the study of the additional constant term γ_q^{ord} , expected to be universal for strip subsystems⁷, only depending on their aspect ratio. It then appeared crucial to impose zero sublattice magnetization in the finite size SW theory, yielding a unique size-dependent staggered field $h^*(L)$ which (i) mimics a tower of state gap $\sim 1/L^2$ in the excitation spectrum (responsible for the logarithmic correction), and (ii) leads to the correct additional geometric constant γ_q^{ord} , in perfect agreement with MG⁷, at least for $q = 2$. A simple and direct relation with non-interacting bosons was also derived. Finally we have precisely investigated the limit of vanishing aspect ratios using very large ladder subsystems in the limit of finite number of legs, discovering that the geometric constant contains both a regular part and a singular component in this limit. Our study is concluded by showing that singular components of even less dominant terms explain perfectly the discrepancy of the area law terms obtained from fixed width *vs.* fixed

aspect ratio subsystems.

Among the potentially interesting future directions, a quantitative study of the geometric constant using exact Monte Carlo, while very challenging, appears to be a very important point in order to test the validity of our prediction for $q > 2$. It may also be interesting to extend the present SW approach to other continuous symmetries like SU(N) models using modified flavor-wave theory for instance. Other geometries or $d = 3$ are certainly of great interest also, with a larger choice of subsystem shapes.

ACKNOWLEDGMENTS

We would like to thank T. Grover, R. Melko, M. Metlitski, and T. Roscilde for discussions. We are grateful to H. Casini for sharing with us the estimates of the corner contributions from Ref. 11. We also want to acknowledge X. Plat for participation in related projects. This work was performed using HPC resources from GENCI (Grant No. x2015050225) and CALMIP (Grant No. 2015-P0677), and is supported by the French ANR program ANR-11-IS04-005-01.

-
- ¹ J. Eisert, M. Cramer, and M. Plenio, “Colloquium: Area laws for the entanglement entropy,” *Rev. Mod. Phys.* **82**, 277 (2010).
- ² Note that systems having a Fermi surface exhibit multiplicative logarithmic corrections to the area law, see for instance D. Gioev and I. Klich, *Phys. Rev. Lett.* **96**, 100503 (2006).
- ³ A. Kitaev and J. Preskill, “Topological Entanglement Entropy,” *Phys. Rev. Lett.* **96**, 110404 (2006).
- ⁴ M. Levin and X.-G. Wen, “Detecting Topological Order in a Ground State Wave Function,” *Phys. Rev. Lett.* **96**, 110405 (2006).
- ⁵ S. Furukawa and G. Misguich, “Topological entanglement entropy in the quantum dimer model on the triangular lattice,” *Phys. Rev. B* **75**, 214407 (2007).
- ⁶ S. V. Isakov, M. B. Hastings, and R. G. Melko, “Topological entanglement entropy of a Bose-Hubbard spin liquid,” *Nature Phys.* **7**, 772 (2011).
- ⁷ M. A. Metlitski and T. Grover, “Entanglement Entropy of Systems with Spontaneously Broken Continuous Symmetry,” [arXiv:1112.5166](https://arxiv.org/abs/1112.5166) (2011).
- ⁸ H. F. Song, N. Laflorencie, S. Rachel, and K. Le Hur, “Entanglement entropy of the two-dimensional Heisenberg antiferromagnet,” *Phys. Rev. B* **83**, 224410 (2011).
- ⁹ B. Kulchytsky, C. M. Herdman, S. Inglis, and R. G. Melko, “Detecting Goldstone Modes with Entanglement Entropy,” [arXiv:1502.01722](https://arxiv.org/abs/1502.01722) (2015).
- ¹⁰ D. J. Luitz, X. Plat, F. Alet, and N. Laflorencie, “Universal logarithmic corrections to entanglement entropies in two dimensions with spontaneously broken continuous symmetries,” *Phys. Rev. B* **91**, 155145 (2015).
- ¹¹ H. Casini and M. Huerta, “Universal terms for the entanglement entropy in dimensions,” *Nuclear Physics B* **764**, 183 (2007).
- ¹² A. B. Kallin, M. B. Hastings, R. G. Melko, and R. R. P. Singh, “Anomalies in the entanglement properties of the square-lattice Heisenberg model,” *Phys. Rev. B* **84**, 165134 (2011).
- ¹³ S. Humeniuk and T. Roscilde, “Quantum Monte Carlo calculation of entanglement Rnyi entropies for generic quantum systems,” *Phys. Rev. B* **86**, 235116 (2012).
- ¹⁴ J. Helmes and S. Wessel, “Entanglement entropy scaling in the bilayer Heisenberg spin system,” *Phys. Rev. B* **89**, 245120 (2014).
- ¹⁵ I. Frérot and T. Roscilde, “Area law or not area law? A microscopic inspection into the structure of entanglement and fluctuations,” [arXiv:1506.00545](https://arxiv.org/abs/1506.00545) (2015).
- ¹⁶ L. Tagliacozzo, G. Evenbly, and G. Vidal, “Simulation of two-dimensional quantum systems using a tree tensor network that exploits the entropic area law,” *Phys. Rev. B* **80**, 235127 (2009).
- ¹⁷ R. R. P. Singh, R. G. Melko, and Jaan Oitmaa, “Thermodynamic singularities in the entanglement entropy at a two-dimensional quantum critical point,” *Phys. Rev. B* **86**, 075106 (2012).
- ¹⁸ A. Kallin, K. Hyatt, R. R. P. Singh, and R. G. Melko, “Entanglement at a Two-Dimensional Quantum Critical Point: A Numerical Linked-Cluster Expansion Study,” *Phys. Rev. Lett.* **110**, 135702 (2013).
- ¹⁹ S. Inglis and R. G. Melko, “Entanglement at a two-dimensional quantum critical point: a t=0 projector quantum monte carlo study,” *New Journal of Physics* **15**, 073048 (2013).
- ²⁰ A. B. Kallin, E. M. Stoudenmire, P. Fendley, R. R. P. Singh, and R. G. Melko, “Corner contribution to the entanglement entropy of an O(3) quantum critical point in 2 + 1 dimensions,” *J. Stat. Mech.* **2014**, P06009 (2014).
- ²¹ E. M. Stoudenmire, P. Gustainis, R. Johal, S. Wessel, and

- R. G. Melko, “Corner contribution to the entanglement entropy of strongly interacting $O(2)$ quantum critical systems in 2+1 dimensions,” *Phys. Rev. B* **90**, 235106 (2014).
- ²² T. Devakul and R. R. P. Singh, “Quantum critical universality and singular corner entanglement entropy of bilayer heisenberg-ising model,” *Phys. Rev. B* **90**, 064424 (2014).
- ²³ T. Devakul and R. R. P. Singh, “Entanglement across a cubic interface in 3 + 1 dimensions,” *Phys. Rev. B* **90**, 054415 (2014).
- ²⁴ J. Helmes and S. Wessel, “Correlations and entanglement scaling in the quantum critical bilayer XY model,” (2014), [arXiv:1411.7773](https://arxiv.org/abs/1411.7773).
- ²⁵ P. Bueno, R. C. Myers, and W. Witczak-Krempa, “Universality of corner entanglement in conformal field theories,” [arXiv:1505.04804](https://arxiv.org/abs/1505.04804) (2015).
- ²⁶ M. Takahashi, “Modified spin-wave theory of a square-lattice antiferromagnet,” *Phys. Rev. B* **40**, 2494 (1989).
- ²⁷ J. E. Hirsch and S. Tang, “Spin-wave theory of the quantum antiferromagnet with unbroken sublattice symmetry,” *Phys. Rev. B* **40**, 4769 (1989).
- ²⁸ P. Chandra and B. Douçot, “Possible spin-liquid state at large S for the frustrated square Heisenberg lattice,” *Phys. Rev. B* **38**, 9335 (1988).
- ²⁹ F. J. Dyson, “General Theory of Spin-Wave Interactions,” *Phys. Rev.* **102**, 1217 (1956).
- ³⁰ S. Maleev, *Sov. Phys. JETP* **6**, 776 (1958).
- ³¹ P. W. Anderson, “An Approximate Quantum Theory of the Antiferromagnetic Ground State,” *Phys. Rev.* **86**, 694 (1952).
- ³² I. Peschel and V. Eisler, “Reduced density matrices and entanglement entropy in free lattice models,” *J. Phys. A: Math. Theor.* **42**, 504003 (2009).
- ³³ L. Bombelli, R. K. Koul, J. Lee, and R. D. Sorkin, “Quantum source of entropy for black holes,” *Phys. Rev. D* **34**, 373 (1986).
- ³⁴ M. B. Plenio, J. Eisert, J. Dreißig, and M. Cramer, “Entropy, Entanglement, and Area: Analytical Results for Harmonic Lattice Systems,” *Phys. Rev. Lett.* **94**, 060503 (2005).
- ³⁵ T. Barthel, M.-C. Chung, and U. Schollwöck, “Entanglement scaling in critical two-dimensional fermionic and bosonic systems,” *Phys. Rev. A* **74**, 022329 (2006).
- ³⁶ M. Srednicki, “Entropy and area,” *Phys. Rev. Lett.* **71**, 666 (1993).
- ³⁷ C. Callan and F. Wilczek, “On geometric entropy,” *Physics Letters B* **333**, 55 (1994).
- ³⁸ E. Fradkin and J. E. Moore, “Entanglement Entropy of 2d Conformal Quantum Critical Points: Hearing the Shape of a Quantum Drum,” *Phys. Rev. Lett.* **97**, 050404 (2006).
- ³⁹ B. Swingle, “Mutual information and the structure of entanglement in quantum field theory,” [arXiv:1010.4038](https://arxiv.org/abs/1010.4038) (2010).
- ⁴⁰ J. Vidal, S. Dusuel, and T. Barthel, “Entanglement entropy in collective models,” *J. Stat. Mech.* **2007**, P01015 (2007).
- ⁴¹ W. Ding, N. E. Bonesteel, and K. Yang, “Block entanglement entropy of ground states with long-range magnetic order,” *Phys. Rev. A* **77**, 052109 (2008).
- ⁴² A. Sen, H. Suwa, and A. W. Sandvik, “Velocity of excitations in ordered, disordered and critical antiferromagnets,” [arXiv:1505.02535](https://arxiv.org/abs/1505.02535) (2015).
- ⁴³ C. J. Hamer, Zheng W., and J. Oitmaa, “Spin-wave stiffness of the Heisenberg antiferromagnet at zero temperature,” *Phys. Rev. B* **50**, 6877 (1994).
- ⁴⁴ O. F. Syljuåsen and A. W. Sandvik, “Quantum Monte Carlo with directed loops,” *Phys. Rev. E* **66**, 046701 (2002).
- ⁴⁵ D. A. Huse, “Ground-state staggered magnetization of two-dimensional quantum Heisenberg antiferromagnets,” *Phys. Rev. B* **37**, 2380 (1988).
- ⁴⁶ A. W. Sandvik, “Finite-size scaling of the ground-state parameters of the two-dimensional Heisenberg model,” *Phys. Rev. B* **56**, 11678 (1997).
- ⁴⁷ R. M. Gray, “Toeplitz and Circulant Matrices: A Review,” *Commun. Inf. Theory* **2**, 155–239 (2005).

Appendix A: Details of spin-wave calculations

This appendix provides details of spin-wave calculations which are not crucial for the computation of entanglement entropy, but which are nonetheless useful for an understanding of the method and its range of validity. We also provide a comparison between the finite-size SW approach and direct QMC computations for $S = 1/2$ for the antiferromagnetic structure factor in the ferromagnetic range of next neighbor coupling $J_2 < 0$.

1. Spin-wave spectrum and velocity

We present in Fig. 13 the spectrum $\Omega_{\mathbf{k}} = 2\sqrt{A_{\mathbf{k}}^2 - B_{\mathbf{k}}^2}$ in the direction $k_x = k_y$ (obtained from expressions Eq. (2.6)) as a function of k_x , for different coupling strengths J_2 and for a spin value $S = 1/2$. The inset represents the spin-wave velocity, Eq. (2.11), as a function of J_2/J_1 . We see that the velocity vanishes at $J_2/J_1 = 0.5$ where the SW spectrum features a continuous line of minima at $k_x = 0$ and $k_y = 0$, as depicted in Fig. 14.

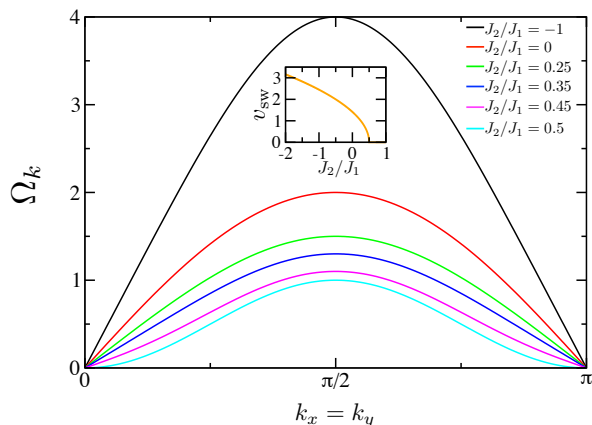


Figure 13. SW spectrum at $h = 0$ for various J_2/J_1 plotted along the $k_x = k_y$ direction. Inset: SW velocity v_{sw} .

2. Range of non-vanishing staggered magnetization

a. Antiferromagnetic order parameter

Eq. (2.12) can be evaluated numerically for different values of the spin size S and second neighbor coupling strength J_2/J_1 , in order to probe the range of validity of the spin-wave approach, which assumes an ordered ground-state. This is illustrated in Fig. 15 where the AF order parameter is represented, and as expected, is clearly enhanced by ferromagnetic diagonal coupling $J_2/J_1 < 0$ while it decreases towards zero when J_2/J_1 approaches $1/2$. The critical frustration J_2^c (in units of

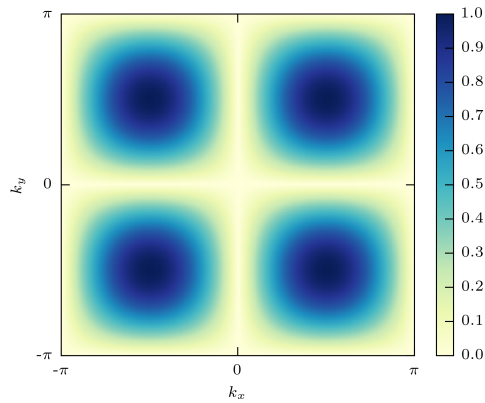


Figure 14. 2D color map of the SW spectrum at $h = 0$ for $J_2/J_1 = 1/2$ and $S = 1$. A line of minima is visible along the $k_x = 0$ and $k_y = 0$ directions.

J_1), above which the SW-corrected order parameter vanishes, is also represented in the inset of Fig. 15 as a function of S where we observe that $J_2^c \rightarrow 1/2$ when S gets larger.

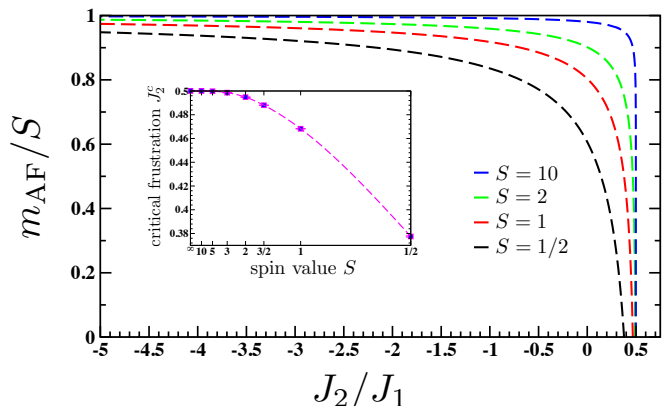


Figure 15. SW results for the AF order parameter Eq. (2.12) of the $J_1 - J_2$ model on the square lattice for various spin sizes S . Inset: Critical frustration J_2^c (in units of J_1) plotted against the spin length S .

b. Finite size SW: AF structure factor

To illustrate the interest of using a formulation of SW which treats more correctly finite-size systems, we present results for the computation of the staggered structure factor per site on finite square lattices $L \times L = N$:

$$s(\pi, \pi) = \frac{1}{N^2} \sum_{ij} (-1)^{|i-j|} \langle \mathbf{S}_i \cdot \mathbf{S}_j \rangle. \quad (\text{A1})$$

Using Wick's theorem, all two-spin correlators can be computed in terms of the f_{ij} and g_{ij} functions defined in

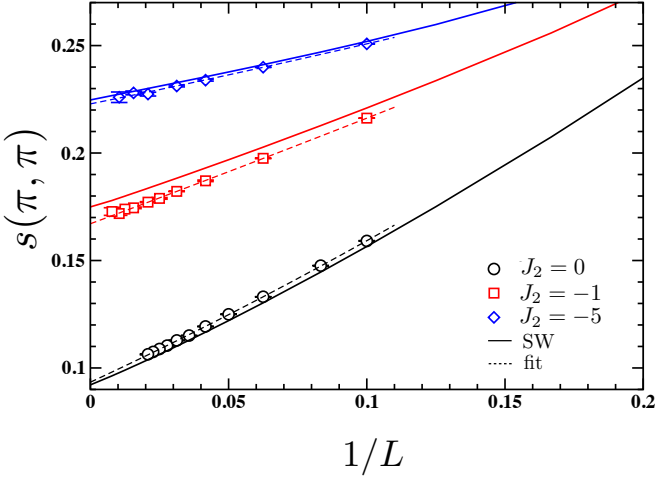


Figure 16. Staggered structure factor per site $s(\pi, \pi)$ of the $J_1 - J_2$ antiferromagnet Eq. (1.5) plotted against the inverse system length $1/L$ for 3 values of J_2 , with $J_1 = 1$. Symbols show $T = 0$ QMC results, dashed lines are quadratic fits of the form Eq. (A3), and the full lines are modified SW results using Eq (A2).

Eq. (2.20) of the main text. Imposing that $\langle \mathbf{S}_i \cdot \mathbf{S}_j \rangle = \langle S_i^z S_j^z \rangle$ (because the theory is strictly speaking not rotationally invariant), we obtain:

$$s(\pi, \pi) = \frac{1}{N^2} \sum_{ij} (f_{ij}^2 + g_{ij}^2) - \frac{1}{4N}. \quad (\text{A2})$$

A quantitative comparison between the above SW expectation and exact quantum Monte Carlo simulations is shown in Fig. 16. Ground-state expectation values for $s(\pi, \pi)$ of the $J_1 - J_2$ Hamiltonian Eq. (1.5) with $S = 1/2$ and $J_2 = 0, -1, -5$ have been obtained for various square lattices $L \times L$ using the stochastic series expansion algorithm⁴⁴. One sees in Fig. 16 that the agreement is fairly good, in particular for strong second neighbor ferromagnetic coupling $J_2/J_1 = -5$. Interestingly, the finite size scaling behavior, expected from previous works^{45,46}

$$s(\pi, \pi) = m_{\text{AF}}^2 + m_1/L + m_2/L^2 + \dots \quad (\text{A3})$$

is very well captured by SW calculations, as visible in Table IV where QMC and SW estimates for m_{AF} , m_1 , and m_2 are compared and show a good agreement.

J_2/J_1	m_{AF}^2	m_1	m_2
	SW / QMC	SW / QMC	SW / QMC
0	0.092 / 0.093(1)	0.55 / 0.60(1)	0.8 / 0.6(1)
-1	0.175 / 0.167(1)	0.42 / 0.47(2)	0.4 / 0.15(9)
-5	0.225 / 0.223(1)	0.25 / 0.26(2)	0.2 / 0.2(1)

Table IV. Fit parameters from Eq. (A3).

The fact that finite size corrections are well captured by this modified SW formalism is a confirmation that it

is a good starting point to study ground-state properties on finite systems and in particular the finite size scaling of the entanglement entropy, as discussed in the main text.

Appendix B: Mean-field limit

In the limit $-J_2/J_1 \gg 1$ one should recover the mean-field result obtained for example for the Lieb-Mattis model^{40,41}. In such a limit, perfect ferromagnetic correlations between spins belonging to the same sublattice imply $f_{ij} = S$ for $i \neq j$ both on the same sublattice ($g_{ij} = 0$) and $f_{ii} = S + 1/2$. Antiferromagnetic correlations between opposite sublattices yield

$$\sum_{ij} f_{ij} - g_{ij} = 0, \quad (\text{B1})$$

thus leading to $g_{ij} = S + 1/N$ for $i \neq j$ on opposite sublattices ($f_{ij} = 0$). Therefore non-zero matrix elements of the correlation \mathbf{C} (for i and j on the same sublattice) are given by

$$\begin{aligned} C_{ii} &= S(1 - r_\Omega) + \frac{1}{4} \\ C_{ij} &= S(1 - r_\Omega), \end{aligned} \quad (\text{B2})$$

where $r_\Omega = N_\Omega/N$ is the ratio between the number of sites inside the sub-system N_Ω and the total number of sites N . The spectrum of the correlation matrix \mathbf{C} is

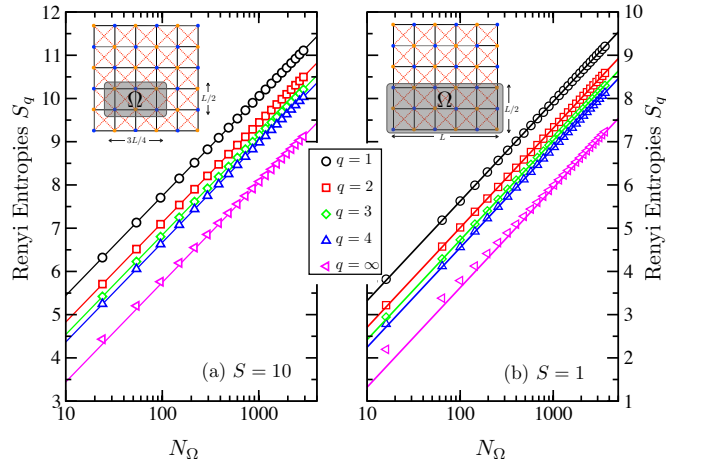


Figure 17. Mean-field limit for the Rényi entropies S_q . The symbols show numerical results for $J_2/J_1 = -10^5$ with different geometries and spin lengths ($S = 1, 10$), plotted against the number N_Ω of sites in the subsystem Ω . The numerical results (symbols) are compared to the analytical expression Eq. (B5) with $r_\Omega = 3/8$ (a) or $r_\Omega = 1/2$ (b), shown by the full lines.

then straightforwardly given by

$$\nu_{1,2}^2 = \frac{N_\Omega}{2} S(1 - r_\Omega) + \frac{1}{4} \quad (\text{B3})$$

$$\nu_l^2 = \frac{1}{4}, \quad (l = 3, \dots, N_\Omega). \quad (\text{B4})$$

one sees that only two eigenvalues contribute, in a macroscopic way. We then compute directly the Rényi entropies for any partition N_Ω and any $q \geq 1$

$$S_q = \ln(N_\Omega) + \ln \left[\frac{S(1 - r_\Omega)}{2} \right] + 2 \frac{\ln q}{q-1}. \quad (\text{B5})$$

The area law term vanishes, and the dominant scaling is now a pure logarithm of the number of sites N_Ω . This exact expression can be compared to the numerical solution of the SW Hamiltonian for very large negative values of J_2 . In Fig. 17 we show numerical results for $J_2/J_1 = -100000$ for two values of S and two different geometries, which compares extremely well with the MF limit expression Eq. (B5). Note that the lines are not fitting functions. If we try instead to fit to the general form $a_q L + l_q \ln L + b_q + c_q/L + d_q/L^2$, we end up with $a_q \sim 10^{-11}$ and $l_q = 2$.

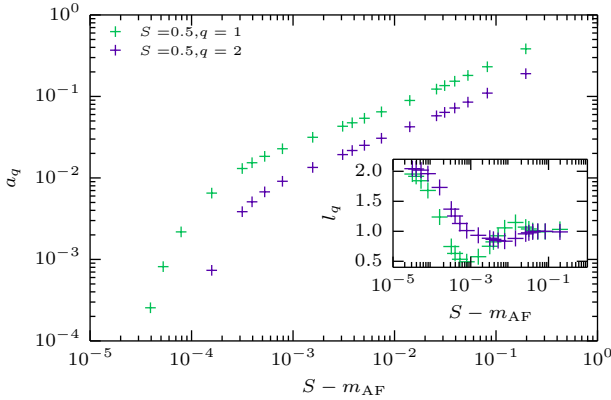


Figure 18. Area law coefficient a_q as a function of the normalized order parameter $S - m_{\text{AF}}$, which is small in the ordered phase. Here, we show results for $S = \frac{1}{2}$. The inset depicts the prefactor of the logarithmic entanglement entropy scaling term, which has a plateau at $l_q = 1$ for intermediate J_2 and evolves to the mean field limit of $J_2 \rightarrow -\infty$. It is unclear if the behavior in the crossover region is a finite size effect or an artefact of the spin wave method.

Before concluding, we want to briefly comment on the crossover to the MF limit when the ferromagnetic second neighbour is turned on towards very large values. This is illustrated in Fig. 18 where the rapid decrease of the area law coefficient a_q (for $q = 1, 2$) is shown versus the quantum depletion of the AF order parameter $S - m_{\text{AF}}$. In the same time, the log coefficients l_1 and l_2 , plotted in the inset of Fig. 18, crossover from $l_q = 1$ up to $l_q = 2$ in the limit of vanishing quantum fluctuations $m_{\text{AF}} \rightarrow S$.

Appendix C: Analytical derivation for one-dimensional subsystems

A great simplification for the computation of entanglement entropy is possible if all sites i and j inside a subsystem Ω are equivalent, or in other words if the matrix elements C_{ij} only depend on the relative distance $|\mathbf{r}_i - \mathbf{r}_j|$. In such a case, for sites on different sublattices $C_{ij} = 0$. This situation is achieved for one-dimensional subsystems with one or two lines (Fig. 1 (a) with $\ell = 1, 2$). In these specific situations, we can derive analytic expressions for the eigenvalues of \mathbf{C} , avoiding a numerical diagonalization. This has first been discussed in Ref. 10, and we provide here details of this calculation, starting with the case of a line-shaped subsystem.

This subsystem being invariant under translations along the x direction, the functions f_{ij} and g_{ij} defined in Eqs.(2.20) only depend on the distance $x = x_i - x_j$ along the subsystem. They reduce consequently to

$$\begin{aligned} f_x &= \frac{1}{2N} \sum_{k_x} \cos(k_x x) \alpha_{k_x}, \\ g_x &= \frac{1}{2N} \sum_{k_x} \cos(k_x x) \beta_{k_x} \end{aligned} \quad (\text{C1})$$

with

$$\alpha_{k_x} := \sum_{k_y} \frac{A_{\mathbf{k}}}{\Omega_{\mathbf{k}}} \quad \text{and} \quad \beta_{k_x} := \sum_{k_y} \frac{B_{\mathbf{k}}}{\Omega_{\mathbf{k}}} \quad (\text{C2})$$

which satisfy the property $\alpha_{k_x + \pi} = \alpha_{k_x}$, $\beta_{k_x} = -\beta_{k_x + \pi}$. Since the functions f_x and g_x possess translation and reflection symmetries

$$f_x = f_{L-x} = f_{L+x}, \quad \text{and} \quad g_x = g_{L-x} = g_{L+x}, \quad (\text{C3})$$

so does the correlation matrix: $C_{ij} = C(l = |x_i - x_j|) = C(L - l) = C(l - L)$. Since furthermore $C(x)$ vanishes for odd distances, it is convenient to re-index all sites on one sublattice from 1 to $L/2$ (say, blue sites in Fig. 1a for $\ell = 1$), and sites on the other sublattices from $L/2 + 1$ to L (say, orange sites in Fig. 1a) to block-diagonalize \mathbf{C} onto two identical blocks of size $L/2 \times L/2$. The translation invariance ensures that each block is *circulant*, with matrix elements $C(l) = \sum_{x \text{ even}} f_x f_{x-l} - \sum_{x \text{ odd}} g_x g_{x-l}$. The eigenvalues ν_l^2 of \mathbf{C} are given by the properties of circulant matrices⁴⁷:

$$\begin{aligned} \nu_l^2 &= c(0) + (-1)^l c\left(\frac{L}{2}\right) + \sum_{j=1}^{\lceil L/4 - 1 \rceil} c(2j) \cos\left(\frac{4\pi}{L} jl\right), \\ l &\in \{0, 1, \dots, \frac{L}{2} - 1\}, \quad c\left(\frac{L}{2}\right) = 0 \quad \text{if} \quad \frac{L}{2} \bmod 2 = 1. \end{aligned} \quad (\text{C4})$$

We can even simplify calculations by noticing that f_x and g_x are discrete Fourier transforms of α_k and β_k respectively. Using the convolution theorem on $C(l)$, we

arrive at the final expression for the L eigenvalues of \mathbf{C} of the *single-line* subsystem:

$$\nu_q^2 = \frac{1}{4N}(\alpha_q^2 - \beta_q^2), \quad (\text{C5})$$

with $q \in \{-\pi + \frac{2\pi}{L}, \dots, \pi\}$.

A very similar reasoning can be applied to the case of a 2-line (ladder) subsystem with $2L$ sites ($\ell = 2$ in Fig. 1a). It is convenient to re-index sites by labelling (in a zig-zag fashion) all (say, blue in in Fig. 1a) sites of one sublattice from 1 to L , and (orange in Fig. 1a) sites from the other sublattice from $L + 1$ to $2L$. Again, \mathbf{C} is block-diagonal with identical circulants blocks with matrix elements $C(l) = \sum_{x=0}^{L-1} f_x^+ f_{x-l}^+ - \sum_x \tilde{g}_x^+ \tilde{g}_{x-l}^+$ with $f_x^+ = f(x, 0) + f(x, 1)$ and $g_x^+ = g(x, 0) + g(x, 1)$. We

can now introduce the discrete Fourier transforms of the newcomers $f(x, 1)$ and $g(x, 1)$

$$\tilde{\alpha}_k := \sum_{k_y} \frac{A_{\mathbf{k}} \cos(k_y)}{\Omega_{\mathbf{k}}} \quad \text{and} \quad \tilde{\beta}_k := \sum_{k_y} \frac{B_{\mathbf{k}} \cos(k_y)}{\Omega_{\mathbf{k}}} \quad (\text{C6})$$

to again be able to apply the convolution theorem. We finally obtain that the L eigenvalues of *one block* of \mathbf{C} for the *ladder* subsystem are given by:

$$\nu_q^2 = \frac{1}{4N} \left[(\alpha_q - \tilde{\alpha}_q)^2 - (\beta_q - \tilde{\beta}_q)^2 \right], \quad (\text{C7})$$

with $q \in \{-\pi + \frac{2\pi}{L}, \dots, \pi\}$. Since \mathbf{C} has two identical blocks, the $2L$ eigenvalues for the ladder subsystem are obtained by doubling the above spectrum.